Simulated Sea Surface Salinity Variability in the Tropical Indian Ocean

Rashmi Sharma, Neeraj Agarwal,* Imran M. Momin, Sujit Basu, and Vijay K. Agarwal[+]

Atmospheric and Oceanic Sciences Group, Space Applications Centre, Ahmedabad, India

ABSTRACT

A long-period (15 yr) simulation of sea surface salinity (SSS) obtained from a hindcast run of an ocean general circulation model (OGCM) forced by the NCEP–NCAR daily reanalysis product is analyzed in the tropical Indian Ocean (TIO). The objective of the study is twofold: assess the capability of the model to provide realistic simulations of SSS and characterize the SSS variability in view of upcoming satellite salinity missions. Model fields are evaluated in terms of mean, standard deviation, and characteristic temporal scales of SSS variability. Results show that the standard deviations range from 0.2 to 1.5 psu, with larger values in regions with strong seasonal transitions of surface currents (south of India) and along the coast in the Bay of Bengal (strong Kelvin-wave-induced currents). Comparison of simulated SSS with collocated SSS measurements from the National Oceanographic Data Center and Argo floats resulted in a high correlation of 0.85 and a root-mean-square error (RMSE) of 0.4 psu. The correlations are quite high (>0.75) up to a depth of 300 m. Daily simulations of SSS compare well with a Research Moored Array for African–Asian–Australian Monsoon Analysis and Prediction (RAMA) buoy in the eastern equatorial Indian Ocean (1.5°S, 90°E) with an RMSE of 0.3 psu and a correlation better than 0.6. Model SSS compares well with observations at all time scales (intraseasonal, seasonal, and interannual). The decorrelation scales computed from model and buoy SSS suggest that the proposed 10-day sampling of future salinity sensors would be able to resolve much of the salinity variability at time scales longer than intraseasonal. This inference is significant in view of satellite salinity sensors, such as *Soil Moisture and Ocean Salinity* (*SMOS*) and Aquarius.

1. Introduction

Ocean salinity, along with ocean temperature and surface wind, controls the dynamic and thermodynamic behavior of the ocean. It also plays an important role in controlling the mixed layer depth variations, especially at low latitudes, in regions of heavy precipitation (Sprintall and Tomczak 1992; Murtugudde and Busalacchi 1998; Han et al. 2001). In such regions, with near-surface haline stratification, salinity is known to influence the evolution of mixed layer temperature indirectly (Rao and Sanil Kumar 1991; Rao and Sivakumar 1999; Howden and Murtugudde 2001). Knowledge of salinity variations is also vital for understanding the ocean hydrological cycle, a key component of the climate system (Webster 1994).

Salinity also affects the Indian monsoon. This connection was first shown by Sanilkumar et al. (1994) from an analysis of the measurements of surface meteorological fields and near-surface salinity structure at the head of the bay during the Monsoon Trough Boundary Layer Experiment in 1990 (MONTBLEX-90). Masson et al. (2005) suggested, from a coupled general circulation model (CGCM) experiment, that there is a link between the spatial structure of the salinity in the southeastern Arabian Sea (SEAS) and the onset of the summer monsoon. In an investigation related to the formation of the Arabian Sea mini warm pool, Vinayachandran et al. (2007) showed that the low-salinity water advected from the Bay of Bengal (BOB) into the SEAS is one of the reasons for the warming of the SEAS. In more recent times, Seo et al. (2009) investigated the effect of freshwater forcing from river discharge into the Indian Ocean on oceanic vertical structure and the Indian monsoon using a regional coupled model. They found that there is a highly seasonal influence of salinity and barrier layer

* Current affiliation: Max Planck Institute for Meteorology, Hamburg, Germany.

[+] Current affiliation: Bhaskaracharya Institute for Space Applications and Geo-Informatics, Gandhinagar, India.

Corresponding author address: Sujit Basu, Space Applications Centre, Ahmedabad 380015, India.
E-mail: rumi_jhim@yahoo.com

on oceanic vertical stratification, which is in turn linked to changes in SST, surface winds, and precipitation.

Despite this importance, there have been relatively few studies on salinity variability in the tropical Indian Ocean (TIO), covering the area 30°S–30°N, 40°–100°E. Earlier studies (Sprintall and Tomczak 1992; Donguy and Meyers 1996; Hareeshkumar and Mathew 1997; Prasanna Kumar and Prasad 1999) analyzed various aspects of sea surface salinity (SSS) variability in this region using scattered datasets. Rao and Sivakumar (2003) used an extensive database to characterize and explain the observed seasonal variability of SSS in the northern Indian Ocean in greater detail. More recently, Delcroix et al. (2005) have used an exhaustive compilation of SSS data collected in the three tropical oceans for determining the time and space scales of the data.

Numerical ocean circulation models have the distinct advantage of generating long time series of salinity at regular spatial and temporal intervals. With increasing accuracy of the forcing data obtained from numerical weather prediction models as well as from satellite observations, the models have attained a high degree of sophistication and are able to provide quite realistic simulations of oceanic parameters including salinity. Han and McCreary (2001) and Han et al. (2001) simulated the SSS of the TIO and studied the influence of salinity on dynamics, thermodynamics and mixed layer physics of the TIO using a 4.5-layer model. The impacts of various precipitation forcings on salinity variability in the TIO were studied using the same model (Perigaud et al. 2003; Sharma et al. 2007). It is also interesting to study the relative importance of different mechanisms in producing the observed variability of SSS in the TIO using an ocean general circulation model (OGCM). Masson et al. (2004) studied the impact of salinity on an Indian Ocean dipole event using such a model. More recently, Thompson et al. (2006) described the variability of salinity in the TIO along with other circulation features in a long-period OGCM simulation. However, they compared their SSS simulations only to climatological variability, and made no attempt to validate the simulation using in situ observations.

In the present work, our focus is on the study of SSS variability at interannual and shorter time scales using an OGCM. A distinctive feature of the study is the validation of the model simulation with available in situ observations. An attempt has also been made to provide insight into the space-based observations, which are available from the recently launched *Soil Moisture and Ocean Salinity* (*SMOS*) mission and will be available from the future Aquarius mission. In this way, our study is similar in spirit to that undertaken by Wang and Chao (2004) in the tropical Pacific.

The paper is organized in the following manner. Section 2 describes the model and data used. Section 3 discusses large-scale features of ocean salinity. Sections 4 and 5 provide detailed comparisons between the model simulations and observations. Section 6 discusses SSS variability in relation to space-based observations. Section 7 provides a summary of the major findings.

2. The model and data

The model used in the present study is the Modular Ocean Model (Pacanowski and Griffies 2000) version 3.1 (MOM3.1), which has been set up for the global domain excluding polar regions (80°S–80°N), with a horizontal resolution varying from 0.5° in the Indian Ocean to 2° in the other oceans. The Indian Ocean resolution is generally adequate to study SSS variability there, as the zonal decorrelation scale for SSS is approximately 4°–7° at 8°–10°N (Delcroix et al. 2005). There are 38 levels in the vertical, with 8 levels in the upper 40 m. The bottom topography is based on $1/12° × 1/12°$ resolution data from the U.S. National Geophysical Data Center. Wind stress is computed from wind velocity using a wind-dependent, drag coefficient (Large and Pond 1982).

The model is initialized with climatological temperature and salinity (Levitus 1982) and is spun up from rest for 60 yr forced by climatological winds (Hellerman and Rosenstein 1983) and with restoring boundary conditions for SST and sea surface salinity. Next, the model is integrated using National Centers for Environmental Prediction–National Center for Atmospheric Research (NCEP–NCAR) daily reanalysis (Kalnay et al. 1996) winds, air temperature, specific humidity, net solar radiation, and net longwave radiation from 1992 to 2006. Latent and sensible heat flux components are computed using the model SST. Daily precipitation data are also from NCEP–NCAR. Monthly climatological river discharge data for 3000 rivers were downloaded from the United Nations Educational, Scientific and Cultural Organization (UNESCO) site for use in the model. The river discharge is distributed as volume transport ($m^3 s^{-1}$), and it is distributed over 2–3 grid points around the river mouths of major rivers. These data are monthly averaged river discharge estimates from Vörösmarty et al. (1998).

Salinity from the top model level (2.5 m) is taken to be SSS. Results are analyzed from 1992 to 2006.

Daily averaged SSS values in the eastern equatorial Indian Ocean (EEIO) from the Research Moored Array for African–Asian–Australian Monsoon Analysis and Prediction (RAMA) buoys are used in the present investigation. RAMA is a key element of the Indian Ocean Observing System (IOOS) program and is a basin-scale moored buoy array. It is designed for studying the
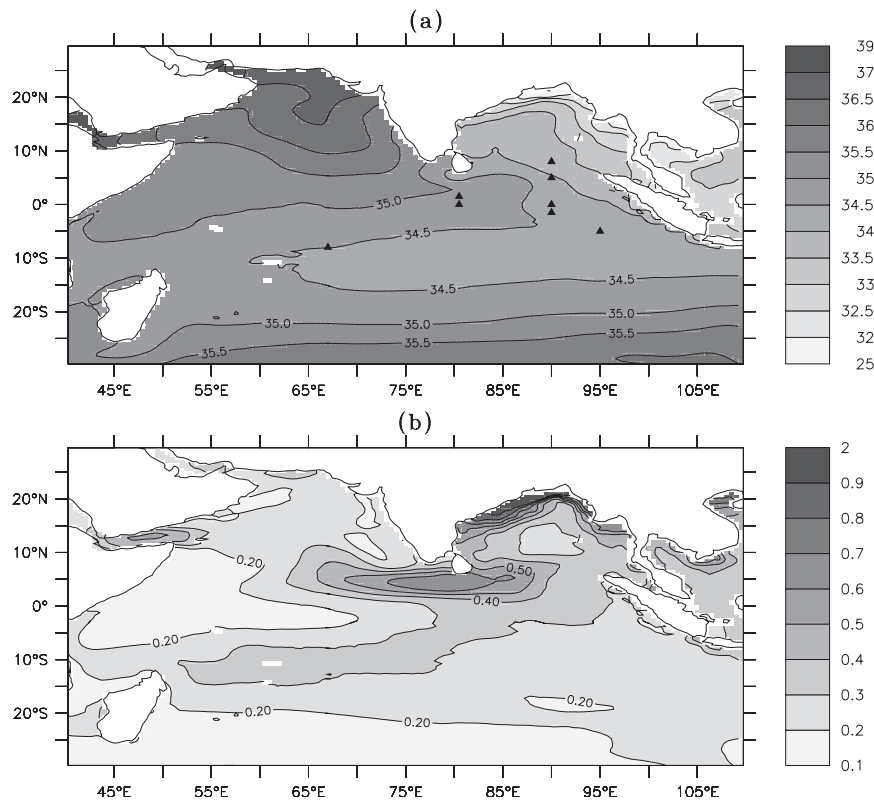
FIG. 1. Simulated (a) mean and (b) standard deviation of SSS (psu) for the TIO. Locations of buoys used in the study are marked with solid triangles in (a).

large-scale ocean–atmosphere interaction, ocean circulation, and mixed layer dynamics. Salinity measured by the buoy at its shallowest depth (1.5 m) and model salinity at 2.5-m depth are considered as SSS in the present study. The validation dataset also consists of salinity profiles from the National Oceanographic Data Center (NODC) and World Ocean Circulation Experiment (WOCE) databases, as well as from Argo profiling float (Argo Science Team 2001) measurements collected between January 2004 and December 2006. Although the Argo data collection began in 2001, very few profiles were collected in the Indian Ocean in the initial years. Because of this reason, the period 2004–06 was selected for comparing model SSS with Argo data. The accuracy of the Argo salinity data is of the order of 0.01 psu (Wong et al. 2003). The shallowest salinity measurements in the Argo database (4–9 m) are considered to be SSS.

3. Large-scale ocean salinity features

We begin our analysis of model SSS with emphasis on the large-scale features of surface salinity over the north Indian Ocean (NIO). Figure 1 shows the mean (1992–2006) and standard deviation of the simulated SSS. Most

of the large-scale features agree with the earlier studies by Rao and Sivakumar (2003) and Donguy and Meyers (1996). The contrasting patterns in the Arabian Sea and Bay of Bengal are quite obvious. In a basin-averaged sense, there is 3–4-psu difference between the two regions. All along the coast in the Bay of Bengal basin, SSS is less than 33.5 psu, primarily because of the combined effect of river discharge and rainfall. Isohaline lines are more closely spaced as one travels northward in the Bay of Bengal. Surface salinity in the Arabian Sea is in excess of 35 psu because of evaporation exceeding precipitation during most of the year. Toward the eastern side of the Arabian Sea, isohaline lines are roughly parallel to the coast with SSS increasing offshore. Along the equator, the zonal gradient is much stronger with an east–west gradient of 0.3×10^{-3} psu km^{-1}.

The standard deviation distribution exhibits strong SSS variability in excess of 1 psu in the coastal regions of the Bay of Bengal, with the variability gradually becoming weaker off the coast. This high-variability region coincides with low mean salinity values. The Bay of Bengal is historically known for comparatively low salinity values, because of excess precipitation over evaporation and also because of heavy river discharge. The
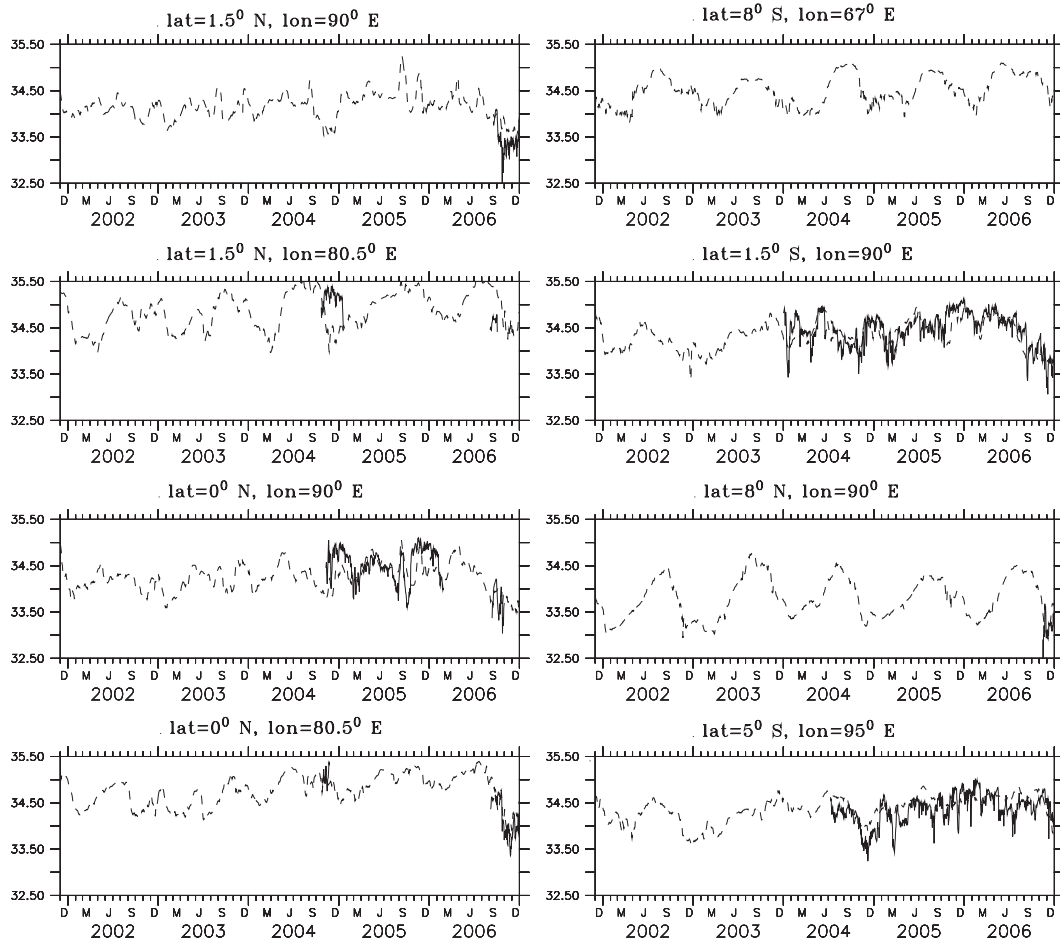
FIG. 2. Modeled (dashed) and observed (solid) daily SSS (psu) at the RAMA buoy locations.

freshwater outflow from rivers is the primary reason for the large variability of SSS along the coasts. Other factors contributing to the SSS variability are the East India Coastal Current (EICC) and coastal Kelvin wave. Another strong variability center lies south of India, where its value exceeds 0.6 psu. This region exhibits strong current variability and wave activity because of the reversing monsoon winds every year. In the Arabian Sea, a small region of moderately high variability can be seen in the Red Sea area. Other parts of the tropical Indian Ocean do not show significant variability, with values in the range of 0.2–0.3 psu.

4. Assessing the model SSS with buoy observations

Figure 2 shows simulated and observed daily SSS for the period 2002–06 at the RAMA buoy locations in the eastern equatorial Indian Ocean (EEIO). One can see that there are large gaps in measurement at practically all the buoys, except for the one located at 1.5°S, 90°E, which measured SSS without much gap from 2004 to

2006. For this reason, we selected this buoy and this particular period for our analyses. Model SSS is in good agreement with buoy SSS, having an RMSE of 0.3 psu and a correlation of 0.62. The mean salinity from observations and model are 34.42 and 34.35 psu, respectively, and the corresponding standard deviations are 0.35 and 0.31 psu. The model slightly underestimates the mean and variability in SSS, and this error could be either due to a deficiency in the NCEP reanalysis product or to unresolved eddy variability.

The RMSE reduces to 0.22 and 0.27 psu for monthly and 10-day-averaged comparisons, respectively. Both accuracies are seemingly worse than the Global Ocean Data Assimilation Experiment (GODAE) requirement of 0.1 psu. The GODAE requirement, however, applies to salinities averaged over a grid of 1° in latitude and 2° in longitude. Since the above errors are obtained at a point location, they will definitely be less when averaged over a 1° × 2° grid. This reduction cannot be confirmed, since unlike the Tropical Atmosphere Ocean
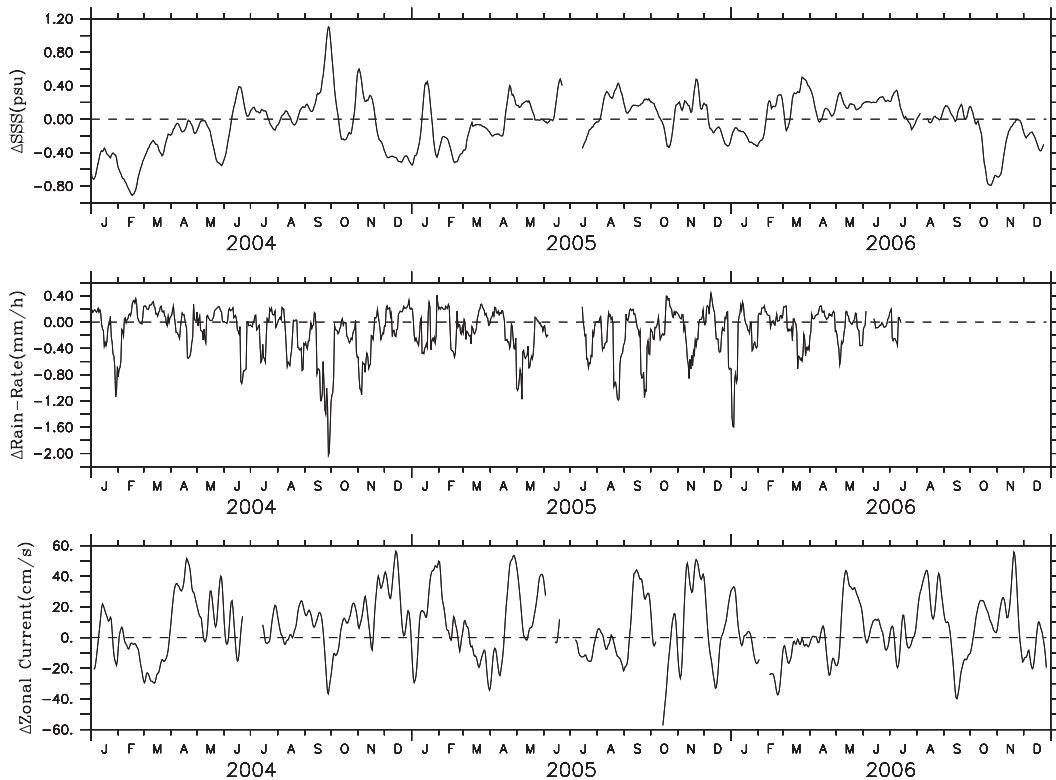
FIG. 3. (top) Difference between modeled and observed SSS, (middle) difference between NCEP and buoy rain rate, and (bottom) difference between model and buoy zonal current. All the differences are shown at the RAMA buoy locations.

(TAO)/Triangle Trans-Ocean Buoy Network (TRITON) array in the equatorial Pacific, there is as yet no such network of buoys in the equatorial Indian Ocean. The model is able to reproduce the interannual variability during this period, especially the low salinity associated with the 2006 dipole event. It is well known that one manifestation of dipole events is a freshening of the upper eastern equatorial Indian Ocean in a narrow region near the Sumatra coast. The observed SSS is less than 33.8 psu during the fall periods of 2004 and 2006, and this freshening is remarkably well reproduced by the model. Though one can see that the model fails to capture transients (isolated peaks and troughs), model SSS can nevertheless be considered reasonably accurate, because it is not adjusted to observed SSS in any way (i.e., by assimilation or relaxation).

Next, we examine the relative effect of precipitation versus advection in explaining model/data SSS differences. For this purpose, buoy-measured zonal current and precipitation data are used. Figure 3 shows the difference between modeled SSS and observed SSS (ΔSSS), along with the difference in precipitation between NCEP and observation and difference in the observed and modeled zonal current. There is no consistent bias in

model SSS at this buoy location. It is clear from the figure that NCEP precipitation is quite weak at this location during the study period. Since NCEP precipitation is so severely underestimated (by more than a factor of 2), local forcing alone would have led to model SSS being far too salty over the entire record, which is not the case. Here advection plays a role in making the surface water less saline than would have been the case if precipitation were the only governing factor in regulating SSS.

Variability of SSS at the RAMA buoy location is also controlled by the surface currents at this location, which are dominated by the strong eastward Wyrtki jets (Wyrtki 1973) that transport high-salinity waters eastward twice a year (March–April and September–October). Wind is the major forcing of these surface currents; hence, the weak wind in the NCEP reanalysis should result in weaker surface currents. This is apparently what happened in the model. As a result, there is a weak transport of salty surface water toward the eastern basin; thus, the surface water at this location remains too fresh, a property that is visible in Fig. 3.

All the above inferences suggest that it is the combined effect of local (precipitation) and nonlocal (advection) forcings that control SSS variability at this
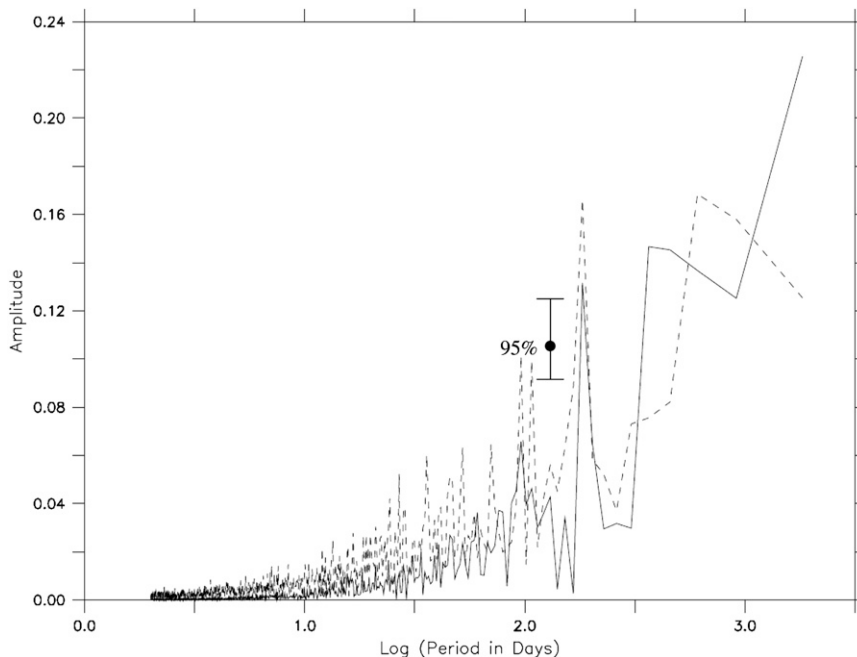
FIG. 4. Fast Fourier transform of modeled (dashed) and observed (solid) SSS at the RAMA
buoy located at 1.5°S, 90°E.

location. The relative effect of these two forcings in controlling the SSS variability over the entire tropical Indian Ocean is discussed later.

We performed a fast Fourier transform analysis on both observed and modeled SSS computed over the period 2004–06 to determine whether the model is able to reproduce the dominant temporal variabilities. Figure 4 shows our results. Both observed and modeled SSS exhibit variability on a wide range of temporal scales. The dominant modes are associated with 90–110 days (at the far end of the intraseasonal band of 20–90 days) and 180 days of periodicity. The latter mode is clearly a manifestation of semiannual periodicity. These peaks have been found to be significant at the 95% confidence level, both in the model and observation. Han (2005) noted that both observed and modeled sea level fields show a dominant 90-day peak. This peak owes its origin to the resonance excitation of the second baroclinic mode waves by the 90-day winds. Shorter-period variability is also captured by the model SSS but with lower power compared to the observations. One possible reason for its low power is that it is produced by precipitation events that are highly localized in space. Thus, the grid size (0.5°) of the model makes the comparison of the model low-period SSS variability a difficult task. Another possibility is that reanalysis precipitation data are known to have uncertainties and are underestimated. In contrast, the high-period SSS variability at this location is controlled by ocean dynamics (largely

advection) and hence is more faithfully reproduced by the model.

Another test of the capability of the model to provide realistic SSS simulations is to compare modeled and observed decorrelation scales Using monthly averaged ship observations of salinity, Delcroix et al. (2005) found the temporal decorrelation scale to be less than 3 months in regions where the seasonal variability is large. In Fig. 5, we show the result of an autocorrelation analysis computed for different time lags. The drop-off of autocorrelation with
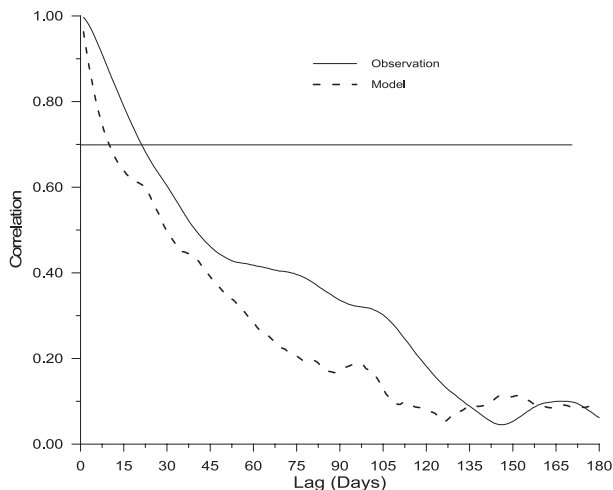

FIG. 5. Autocorrelation of SSS at different lags for model (dashed) and observed (solid) SSS at the RAMA buoy locations.
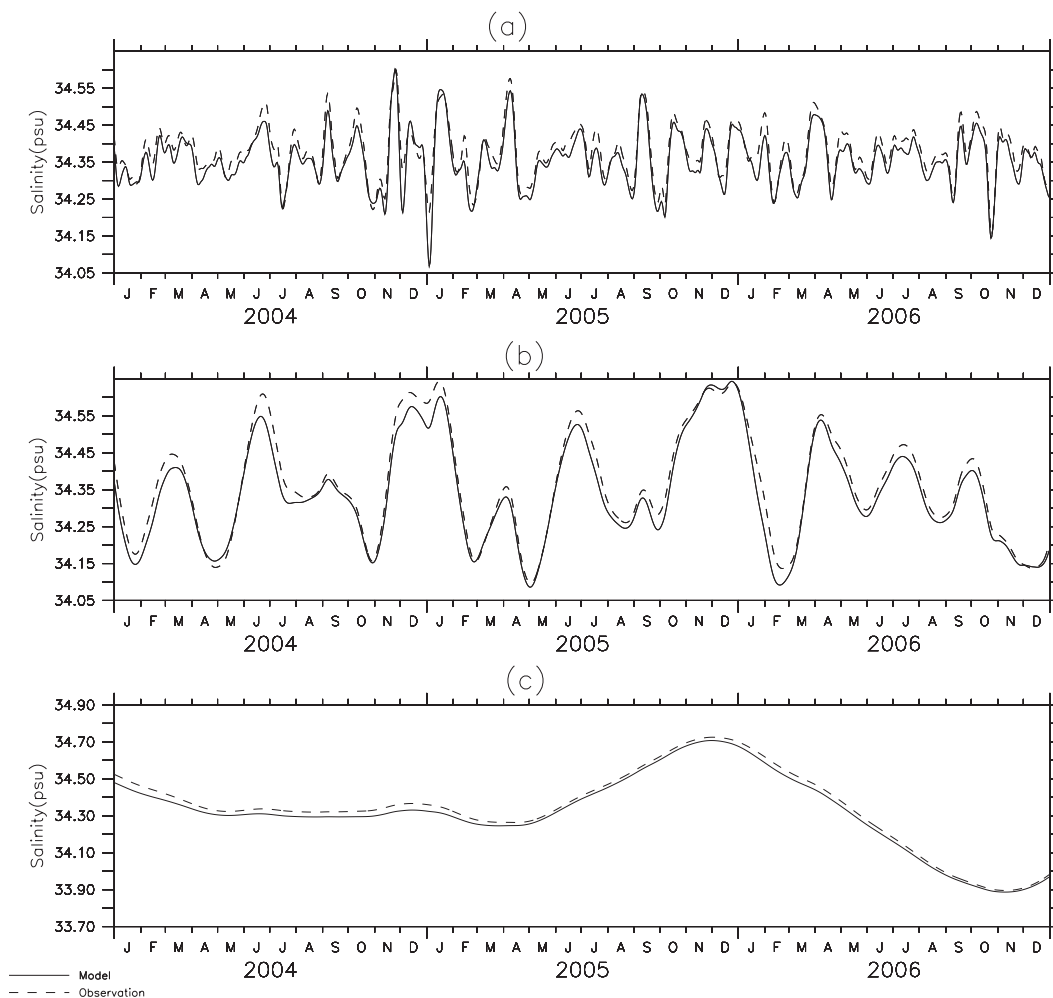
FIG. 6. Filtered SSS at the RAMA buoy locations from model and observations. The filters are for (a) intraseasonal, (b) seasonal, and (c) interannual variability.

time lag is almost the same for both model and observed SSS, *e*-folding times of approximately 15 days for the observed SSS, and approximately 22 days for model SSS. The longer decorrelation scale obtained in the model SSS is possibly due to the model simulation error (because of errors in forcing parameters, intrinsic model error, etc.). The decorrelation scale computed at the buoy location suggests that a 10-day revisit period of a satellite should be sufficient to resolve much of the SSS variability in the EEIO region. A similar analysis for the whole tropical Indian Ocean is discussed in section 6, to confirm that satellite missions, such as *SMOS*, will meet the requirement of the studies on salinity variability in the Indian Ocean.

In the earlier sections, we saw that model salinity compares favorably with observations on synoptic scales. To assess further its capability in simulating SSS variability on other scales (intraseasonal, seasonal, and interannual), we compared model SSS with RAMA buoy measurements in three period bands, namely, 10–60 (intraseasonal), 60–360 (seasonal), and greater than 360 days (interannual). For this purpose a bandpass filter has been used. Figure 6 plots filtered SSS time series from both model and buoy for all the three time scales. There is an excellent match between the model and buoy time series at all the time scales, with correlations better than 0.95 and RMSE less than 0.03 psu. The magnitudes of standard deviation at 10–60 and 60–360 days and at interannual time scales are 0.07, 0.15, and 0.24 psu, respectively, for both model and buoy time series. We conclude that the performance of the model in simulating salinity at these time scales is quite reasonable.

5. Comparison of model SSS with NODC and Argo observations

To compare observed and modeled SSS in the entire NIO, we used SSS data from the National Oceanic and
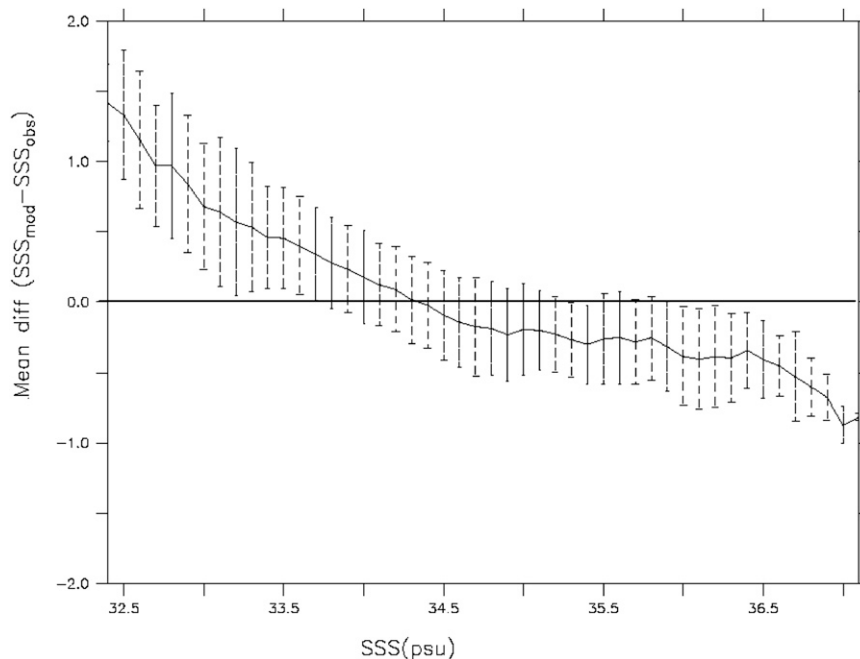
FIG. 7. Binned means of SSS difference as a function of in situ SSS. The outer bars are
±1 std dev.

Atmospheric Administration (NOAA) and Argo for the period January 2004–December 2006. Finding collocated pairs of modeled and observed SSS is always a difficult task because of the different temporal and spatial sampling of the two systems. For temporal collocation, the dates of available observed SSS were examined and SSS from a specific day (which may be just one snapshot realization) was paired with the model SSS (daily averaged) of that day. For spatial collocation, measured profiles falling within the model grid (0.5°) were averaged. This product accounted for 42 000 collocated model–buoy pairs. The comparison produced a correlation coefficient of 0.83 and an RMSE of 0.43 psu. The correlations are quite high (more than 0.75) up to a depth of 300 m. One possible cause of the mismatch may be because the in situ observations are obtained at single points, whereas the model SSS are gridded values representing spatial averages.

Figure 7 shows the binned means and standard deviations of the difference between model and observed SSS for all 42 000 collocations. The differences are divided into bins of 0.1 psu, and the mean and standard deviation are calculated for each bin. It can be seen that the mean values progressively fall with the increasing salinity values. They clearly divide the distribution into two regions, with differences being positive below 34.5 psu and negative above that value. Thus, the model overestimates SSS for low values of salinity, whereas it underestimates SSS for higher values of salinity. It can be clearly seen that model performance is better for higher salinity values, with the

mean difference values and standard deviations of these differences being less. The standard deviations are a bit larger for low-salinity values. These discrepancies could be due to the uncertainties in the NCEP–NCAR precipitation estimates, which were used in the freshwater flux that forced the model. The mean difference of all the observations taken together is 0.1 psu, and the standard deviation is 0.42 psu. Figure 8 presents typical scatterplots of differences between model and in situ SSS as a function of measured SSS for different regions, namely, the Bay of Bengal (10°–20°N, 80°–95°E), eastern equatorial Indian Ocean (10°S−5°N, 70°−100°E), western equatorial Indian Ocean (5°S–10°N, 45°–70°E), and northern Arabian Sea (12°–22°N, 55°–75°E). Note that the model tends to be saltier in the Bay of Bengal, with a mean difference of 0.46 and a standard deviation of 0.6 psu. The model biases are −0.29 and −0.26 psu in the northern Arabian Sea and western equatorial Indian Ocean, respectively. Standard deviations in these two regions are 0.41 and 0.32 psu, respectively, with the model SSS tending to be underestimated. In the eastern equatorial Indian Ocean, there is very little bias (−0.01 psu) in the model simulation.

6. SSS variability in the tropical Indian Ocean: Emphasis on satellite salinity missions

Despite the above-mentioned limitations and errors in the modeled SSS, the simulations can be considered to be reasonably good and can be used for understanding
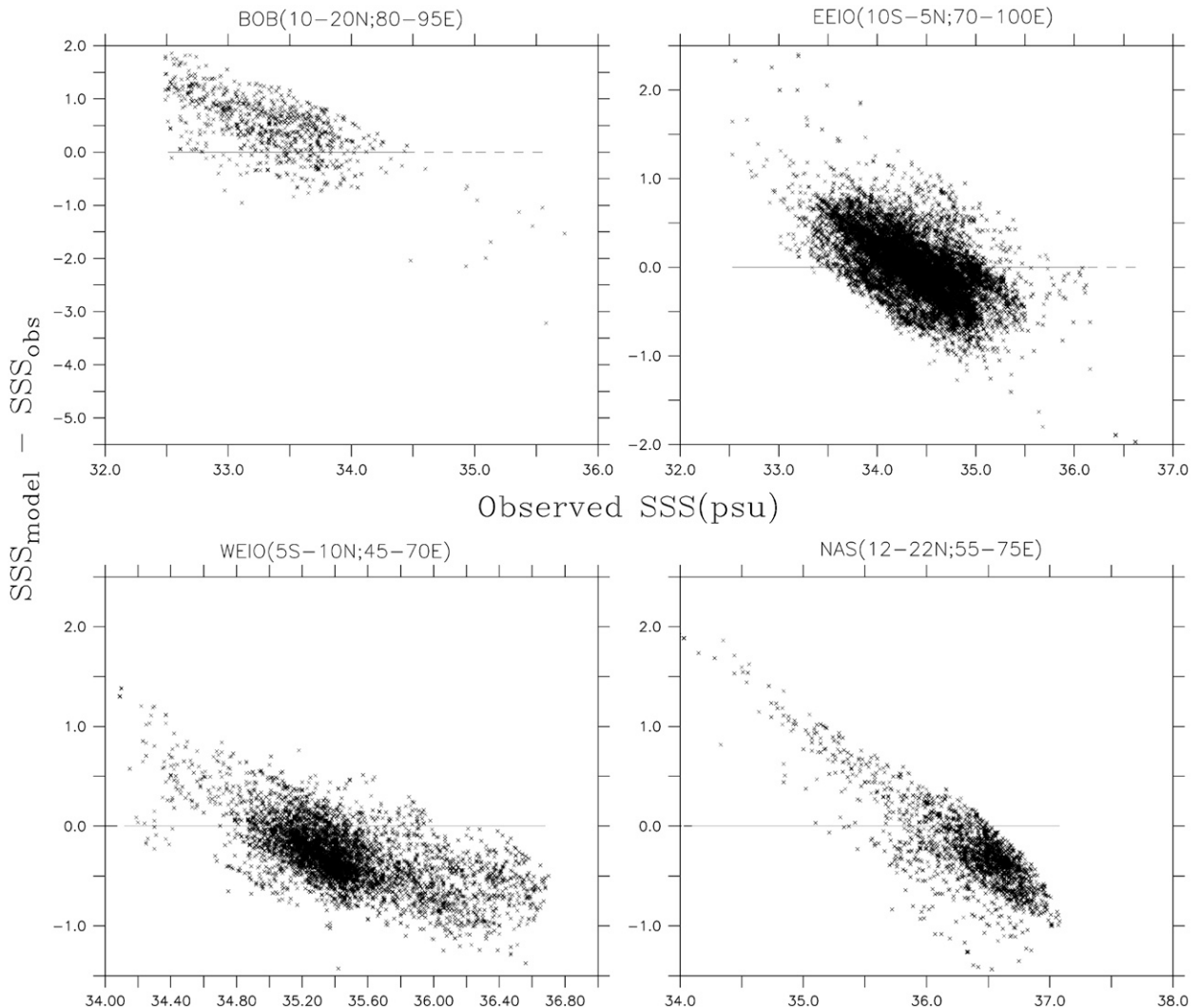
FIG. 8. Scatterplot of SSS differences (model − in situ) as a function of observed salinity for different regions: (a) BOB (10°–20°N, 80°–95°E), (b) EEIO (10°S–5°N, 70°–100°E), (c) western equatorial Indian Ocean (5°S–10°N, 45°–70°E), and (d) northern Arabian Sea (12°–22°N, 55°–75°E).

upper-ocean processes and air–sea interaction. Figure 9 shows decorrelation times for model-simulated SSS over the entire TIO. Except for a few isolated pockets, the times are more than 10 days. The absence of regions with decorrelation scales less than 10 days could be due to a lack of extreme events and the underestimation of high-frequency variability in the model. For an exhaustive investigation of the decorrelation scale over the entire study region, better high-frequency variability in wind, rain, and evaporation should be used in the model. However, as a first approximation, the results of the present study lead to the conclusion that the 10-day sampling of the salinity sensors would be able to resolve much of the SSS variability. We also examined the simulated variability that would be captured by a satellite sensor with

a 10-day sampling period. Accordingly, we computed SSS variability over the Indian Ocean by taking modeled SSS every 10 days. The SSS variability (Fig. 10) ranges between 0.2 and 1.2 psu, with larger variability all along the Bay of Bengal coast (where it exceeds 1 psu) and south of Sri Lanka. The pattern of SSS variability as represented in Fig. 10 essentially matches that shown in Fig. 1, in which the variability was computed using daily simulated SSS. This property again suggests that the 10-day satellite sampling rate is sufficient to resolve most SSS variability.

Having ascertained the model performance at various time scales at the RAMA buoy location, we next examine the distribution of SSS variability in the entire tropical Indian Ocean (Fig. 11). The magnitude of SSS at
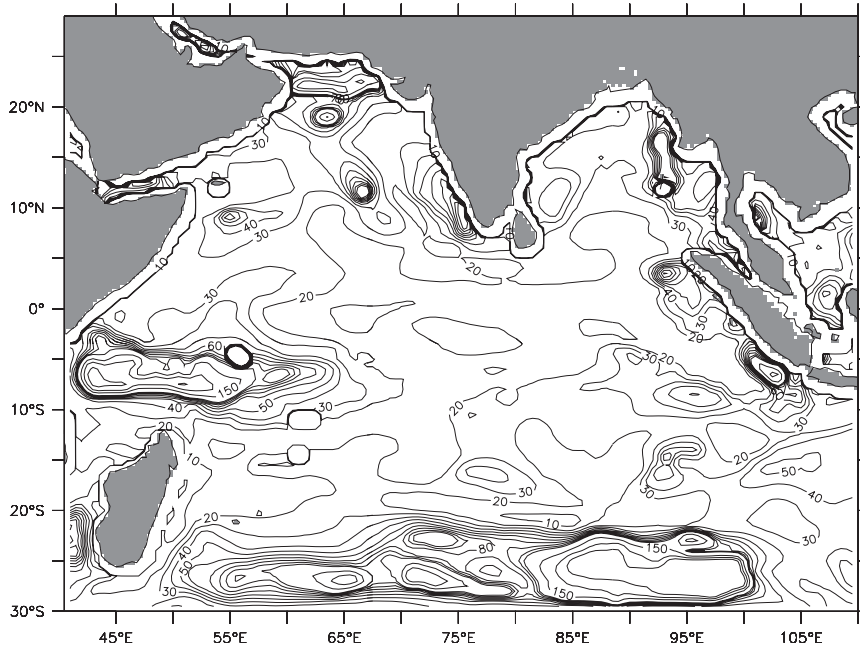
FIG. 9. Spatial distribution of the decorrelation temporal scales (days) for SSS over the TIO.

intraseasonal scale is small, being on the order of 0.02–0.06 psu over a large part of the tropical Indian. On the other hand, the magnitudes of SSS variability at interannual and seasonal scales are large; therefore, they would be easily detected. The northeastern Bay of Bengal is the center of high variability on intraseasonal, seasonal, and interannual time scales. Interestingly, this region happens to be the region of high-salinity gradients. This

variability center is associated with large freshwater discharge from various rivers.

On seasonal and interannual time scales, there is high SSS variability along the periphery of the Bay of Bengal. This variability is associated with the coastal Kelvin wave, which, after reflection from the Sumatra coast, propagates all along the coast of the Bay of Bengal. On interannual time scales, regions north and south of equator
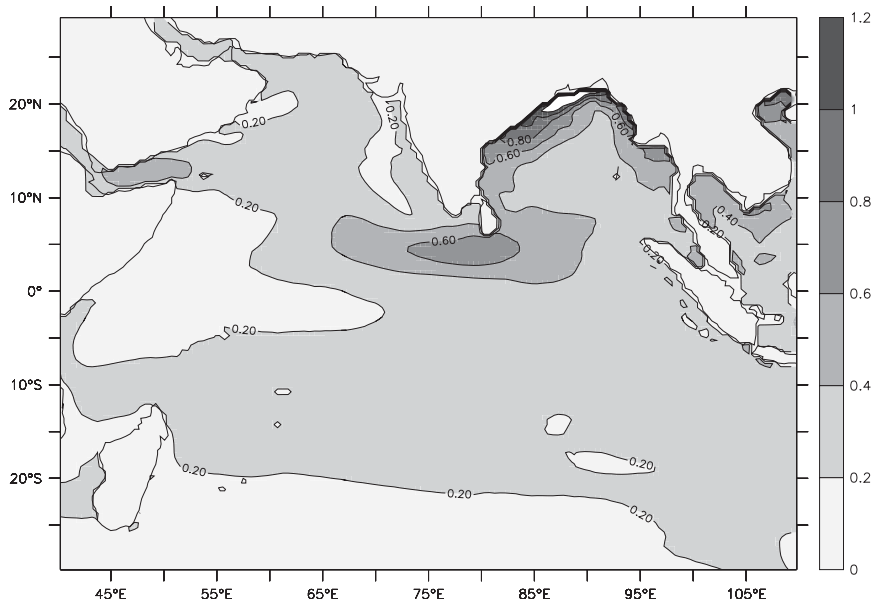
FIG. 10. Model-simulated SSS standard deviation (psu) with a 10-day sampling over the TIO.
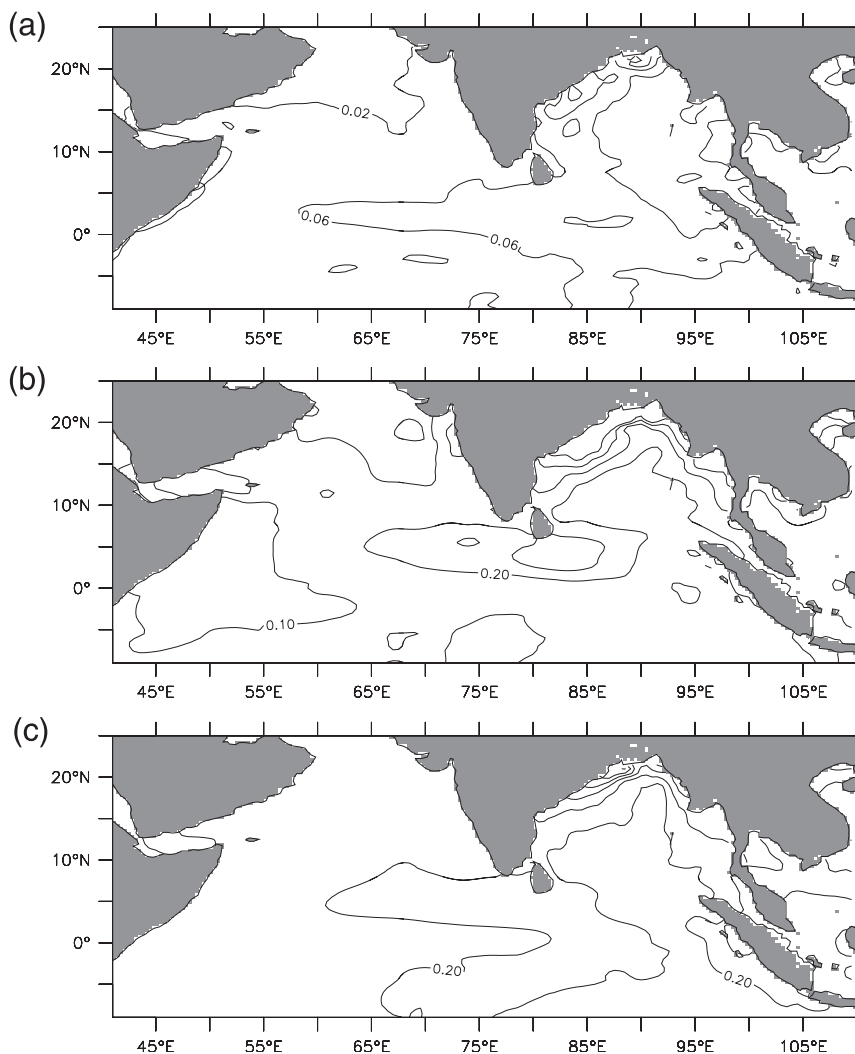
FIG. 11. The standard deviation (psu) of model SSS for 1992–2006 in the entire TIO: (a) 10–60-, (b) 60–360-, and (c) 360-day low-pass filtered.

as well as the region close to Sumatra exhibit large variability (0.2 psu). Along 5°N in the central equatorial region, a large variability center at seasonal time scales can be seen. This center coincides with the strong seasonally reversing zonal currents in this region. At all time scales, the Arabian Sea exhibits low variability. The above inferences suggest that the satellite salinity missions would be able to detect signals on seasonal and interannual time scales in large areas of the tropical Indian Ocean.

7. Summary

The goal of this study is twofold: (i) assess the realism of a simulation of sea surface salinity by an ocean general circulation model forced by NCEP–NCAR

reanalysis products in the tropical Indian Ocean and (ii) study its variability with emphasis on satellite salinity sensors.

The simulated SSS was used to quantify the seasonal cycles of SSS and its variability on different time scales. The spatial distribution of SSS was also studied, and regions of strong variability were identified. The contrasting patterns of SSS in the Arabian Sea and Bay of Bengal were clearly brought out. In particular, the high variability in modeled SSS along the east coast of India was due to the strong East India Coastal Current in combination with significant coastal Kelvin wave activity.

To assess the realism of the simulation of SSS, the simulations were compared with observed salinity. A detailed comparison was carried out using all possible observations available in the study region. A comparison of

modeled and observed SSS from RAMA buoys and Argo/NODC data led to RMSEs of 0.30 and 0.42 psu, respectively. Errors in the model SSS of the order mentioned above could result from a combination of inaccurate forcings, inherent model errors, or errors in collocation. The major forcing for SSS is precipitation. However, the accuracy of its estimation is known to be not quite reliable.

Hence, to fully resolve the issue of SSS variability, a combination of modeled and satellite observed SSS is desirable. In this connection, special emphasis was laid on the relevance of the study for spaceborne sea surface salinity missions. This was done by calculating temporal decorrelation scales in different regions of the tropical Indian Ocean. In almost all the regions, these scales were more than 10 days, suggesting that the 10-day revisit period of the recently launched *SMOS* and future Aquarius satellites should be sufficient to resolve most of the SSS variability in the Indian Ocean.

Thus, the designing strategy of the recently launched *SMOS* satellite has been confirmed by the results reported in the study. It is clear that satellite salinity observation will be able to detect the intraannual to interannual salinity changes. We conclude that, with the SSS data made available in future from such satellites, a more accurate reanalyzed field of the surface salinity can be constructed by blending model simulations and satellite observations on scales longer than intraseasonal scales. Needless to say, the modeling ability to simulate SSS will also be continuously improved once the satellite SSS data are successfully assimilated in the models. The improved reanalysis fields as well as the improved modeling ability will definitely be beneficial for climate-related studies.

REFERENCES

Argo Science Team, 2001: Argo: The global array of profiling floats. *Observing the Oceans in the 21st Century,* C. J. Koblinsky and N. R. Smith, Eds., GODAE Project Office, 248–258.

Delcroix, T., M. J. McPhaden, A. Dessier, and Y. Gouriou, 2005: Time and space scales for sea surface salinity in the tropical oceans. *Deep-Sea Res. I,* **52,** 787–813.

Donguy, J. R., and G. Meyers, 1996: Seasonal variations of sea surface salinity and temperature in the tropical Indian Ocean. *Deep-Sea Res. I,* **43,** 117–138.

Han, W., 2005: Origin and dynamics of the 90-day and 30–60-day variations in the equatorial Indian Ocean. *J. Phys. Oceanogr.,* **35,** 708–727.

——, and J. P. McCreary, 2001: Modeling salinity distributions in the Indian Ocean. *J. Geophys. Res.,* **106,** 859–877.

——, ——, and K. E. Kohler, 2001: Influence of precipitation minus evaporation and Bay of Bengal rivers on dynamics, thermo-dynamics, and mixed layer physics in the upper Indian Ocean. *J. Geophys. Res.,* **106,** 6895–6916.

Hareeshkumar, P. V., and B. Mathew, 1997: Salinity distribution in the Arabian Sea. *Indian J. Mar. Sci.,* **26,** 272–277.

Hellerman, S., and M. Rosenstein, 1983: Normal monthly wind stress over the world ocean with error estimates. *J. Phys. Oceanogr.,* **13,** 1093–1104.

Howden, S. D., and R. Murtugudde, 2001: Effects of river inputs into the Bay of Bengal. *J. Geophys. Res.,* **106,** 19 825–19 843.

Kalnay, E., and Coauthors, 1996: The NCEP/NCAR 40-Year Reanalysis Project. *Bull. Amer. Meteor. Soc.,* **77,** 437–471.

Large, W. G., and S. Pond, 1982: Sensible and latent heat flux measurements over the ocean. *J. Phys. Oceanogr.,* **12,** 464–482.

Levitus, S., 1982: *Climatological Atlas of the World Ocean.* NOAA Prof. Paper 13, 173 pp. and 17 microfiche.

Masson, S., J.-P. Boulanger, C. Menkes, P. Delecluse, and T. Yamagata, 2004: Impact of salinity on the 1997 Indian Ocean dipole event in a numerical experiment. *J. Geophys. Res.,* **109,** C02002, doi:10.1029/2003JC001807.

——, and Coauthors, 2005: Impact of barrier layer on winter-spring variability of the southeastern Arabian Sea. *Geophys. Res. Lett.,* **32,** L07703, doi:10.1029/2004GL021980.

Murtugudde, R., and A. J. Busalacchi, 1998: Salinity effects in a tropical ocean model. *J. Geophys. Res.,* **103,** 3283–3300.

Pacanowski, R. C., and S. M. Griffies, 2000: MOM 3.0 manual. NOAA/Geophysical Fluid Dynamics Laboratory Rep., 680 pp.

Perigaud, C., J. P. McCreary, and K. Q. Zhang, 2003: Impact of interannual rainfall anomalies on Indian Ocean salinity and temperature variability. *J. Geophys. Res.,* **108,** 3319, doi:10.1029/2002JC001699.

Prasanna Kumar, S., and T. G. Prasad, 1999: Formation and spreading of Arabian Sea high-salinity water mass. *J. Geophys. Res.,* **104,** 1455–1464.

Rao, R. R., and K. V. Sanil Kumar, 1991: Evolution of salinity fields in the upper layers of the east central Arabian Sea and northern Bay of Bengal during summer monsoon experiments. *Proc. Indian Acad. Sci.,* **100,** 69–78.

——, and R. Sivakumar, 1999: On the possible mechanisms of the evolution of a mini-warm pool during the pre-summer monsoon season and the onset vortex in the southeastern Arabian Sea. *Quart. J. Roy. Meteor. Soc.,* **125,** 787–809.

——, and ——, 2003: Seasonal variability of sea surface salinity and salt budget of the mixed layer of the north Indian Ocean. *J. Geophys. Res.,* **108,** 3009, doi:10.1029/2001JC000907.

Sanilkumar, K. V., N. Mohankumar, M. X. Joseph, and R. R. Rao, 1994: Genesis of meteorological disturbances and thermohaline variability of the upper layers in the head of the Bay of

Bengal during Monsoon Trough Boundary Layer Experiment (MONTBLEX-90). *Deep-Sea Res. I,* **40,** 1569–1581.

Seo, H., S.-P. Xie, R. Murtugudde, M. Jochum, and A. J. Miller, 2009: Seasonal effects of Indian Ocean freshwater forcing in a regional coupled model. *J. Climate,* **22,** 6577–6596.

Sharma, R., N. Agarwal, S. Basu, and V. K. Agarwal, 2007: Impact of satellite-derived forcings on numerical ocean model simulations and study of sea surface salinity variations in the Indian Ocean. *J. Climate,* **20,** 871–890.

Sprintall, J., and M. Tomczak, 1992: Evidence of the barrier layer in the surface layer of the tropics. *J. Geophys. Res.,* **97,** 7305–7316.

Thompson, B., C. Gnanaseelan, and P. S. Salvekar, 2006: Variability in the Indian Ocean circulation and salinity and its impact on SST anomalies during dipole events. *J. Mar. Res.,* **64,** 854–880.

Vinayachandran, P. N., D. Shankar, J. Kurian, F. Durand, and S. S. C. Shenoi, 2007: Arabian Sea mini warm pool and the monsoon onset vortex. *Curr. Sci.,* **93,** 203–214.

Vörösmarty, C. J., B. Fekete, and B. A. Tucker, cited 1998: River discharge database, version 1.1 (RivDIS v1.0 supplement). [Available online at http://www.rivdis.sr.unh.edu/.]

Wang, X., and Y. Chao, 2004: Simulated sea surface salinity variability in the tropical Pacific. *Geophys. Res. Lett.,* **31,** L02302, doi:10.1029/2003GL018146.

Webster, P. J., 1994: The role of hydrological processes in ocean-atmosphere interactions. *Rev. Geophys.,* **32,** 427–476.

Wong, A., G. Johnson, and W. Owens, 2003: Delayed-mode calibration of autonomous CTD profiling float salinity by θ–S climatology. *J. Atmos. Oceanic Technol.,* **20,** 308–318.

Wyrtki, K., 1973: An equatorial jet in the Indian Ocean. *Science,* **182,** 254–262.